La0.6Sr0.4Fe0.8Co0.2O3-δ electrophoretic coating for oxygen transport membranes

L. Guironnet, P.-M. Geffroy, F. Jouay, C. Pagnoux, N. Richet, T. Chartier

$La_{0.6}Sr_{0.4}Fe_{0.8}Co_{0.2}O_{3-\delta}$ electrophoretic coating for oxygen transport membranes

L. Guironnet[1,3], P.-M. Geffroy[1,*], F. Jouay[1], C. Pagnoux[1], N. Richet[2], T. Chartier[1]

[1]*IRCER, CNRS, Université de Limoges. CEC. 12 Rue Atlantis 87068 Limoges. France*
[2]*Air Liquide CRCD, 1 chemin de la Porte des Loges, BP126, 78354 Jouy en Josas, France*
[3]*ADEME, 20 rue du Grésillé – BP90406, 49004 Angers Cedex 01, France*

***Corresponding Author: Pierre-Marie Geffroy**
Affiliation: IRCER, CNRS, Université de Limoges, CEC,
Address: 12 rue Atlantis 87068 Limoges, France,
Phone: **05 87 50 23 53,**
Fax: **05 87 50 23 04,**
E-mail : pierre-marie.geffroy@unilim.fr

Key words: electrophoretic coating, oxygen semi-permeation, porous layer, mixed conductor

Abstract

This work describes the development of electrophoretic deposition method for the elaboration of a porous coating on a dense membrane in order to improve its oxygen permeation performance. The dense membrane material produced from $La_{0.5}Sr_{0.5}Fe_{0.7}Ga_{0.3}O_{3-\delta}$ perovskite is coated with $La_{0.6}Sr_{0.4}Fe_{0.8}Co_{0.2}O_{3-\delta}$ perovskite layer by electrophoretic deposition method in order to improve the kinetics of oxygen surface exchanges. Then, the oxygen flux through the $La_{0.5}Sr_{0.5}Fe_{0.7}Ga_{0.3}O_{3-\delta}$ dense membrane is largely impacted by $La_{0.6}Sr_{0.4}Fe_{0.8}Co_{0.2}O_{3-\delta}$ electrophoretic coating, from 0.5 to 2.6 10^{-3} $mol.m^{-2}.s^{-1}$ without and with $La_{0.6}Sr_{0.4}Fe_{0.8}Co_{0.2}O_{3-\delta}$ coating after heating at 900°C, respectively. Besides, a large impact of the thickness of the electrophoretic coating on the oxygen flux through the membranes is observed. The electrophoretic deposition has shown to be a powerful elaboration method of membrane to produce gaseous oxygen with high purity.

1. Introduction

The oxygen transport membrane (OTM) are dense ceramic membranes produced from mixed ionic and electronic conducting materials. One of the advantages of this technology is the high purity of the gaseous oxygen produced (higher than 99%). The technology could be interesting to use for laser cutting process [Powell, 2019]. However, oxygen transport membranes must have a high oxygen semi-permeation for industrial applications. The electromotive force of the oxygen transport through the membranes comes from the difference of oxygen partial pressure of the two atmospheres on both membrane sides. Unfortunately, the oxygen flux

through the membrane is usually limited by the oxygen surface exchanges [Geffroy 2015, Geffroy 2017], and a coating of submicronic particles on the dense membrane can lead to improve the kinetics of the oxygen surface exchanges and then improve oxygen flux [Hayamizu 2014, Xu 1999].

In this context, this work is focused on the impact of the thickness of a surface porous layer deposited by electrophoretic deposition on a membrane, using submicronic particles, on the oxygen flux performance. $La_{0.5}Sr_{0.5}Fe_{0.7}Ga_{0.3}O_{3-\delta}$ ($LSFG_{5573}$) perovskite is used as dense membrane material because of its high oxygen diffusion coefficient, good chemical stability and mechanical properties [Sunaro 2008, Geffroy 2013]. $La_{0.6}Sr_{0.4}Fe_{0.8}Co_{0.2}O_{3-\delta}$ ($LSFCo_{6482}$) perovskite, with very high kinetics for oxygen surface exchanges [Guironnet 2016] but low mechanical properties, is used as coating materials onto the membrane, in order to improve the kinetics of oxygen surface exchanges. The coating on the dense membrane is manufactured by electrophoretic deposition (EPD). This coating method has a great interest because it can be used for many different materials. The main advantages of electrophoretic deposition is a short coating time, easy control of films thickness (from few microns to several hundred microns), low cost, possibility of mass production and suitable for substrates with complex shape as tubular [Zhang 2007, Tan 210, Schulz 2010].

Electrophoresis coating method requires to prepare a dispersed suspension of ceramic particles. These ceramic particles should exhibit electrical surface charge to move in a solvent under an electric field applied between the electrode and the substrate. Then, particles coagulate onto the substrate to form a layer. The nature of the surface charges on the ceramic particles determine if the coating is cathodic or anodic. The properties of the coating mainly depend on the characteristics of the ceramic suspension [Boccaccini 2002, Zhitomirsky 2000, Heavens 1990, Hammaker 1940].

The electrophoretic coating shows recently a great interest for the preparation of thin porous coating in electrochemical systems, in particular for the elaboration of electrode in solid oxide fuel cell [Majhi 2011]. This work shows the impact of electrophoretic coating on the electrochemical properties of mixed conductor membranes.

2. Experimental

2.1 Materials

The powders used in this study are synthesized by a solid state reaction synthesis [Etchegoyen 2006] for $La_{0.5}Sr_{0.5}Fe_{0.7}Ga_{0.3}O_{3-\delta}$ ($LSFG_{5573}$) powder and by a citrate route [Xu 2004] for $La_{0.6}Sr_{0.4}Fe_{0.8}Co_{0.2}O_{3-\delta}$ ($LSFCo_{6482}$) powder.

$LSFG_{5573}$ powder used for the membrane preparation is synthetized from pure oxides (La_2O_3 (99.99 %, Alfa Aesar), Fe_2O_3 (98 %, Alfa Aesar), Ga_2O_3 (99.999 %, Alfa Aesar)) dehydrated at 100°C. Then oxides and carbonate ($SrCO_3$ (99.9 %, Sigma-Aldrich)) precursors are weighed in proper amount, mixed and attrition-milled at 600 rpm in ethanol. The attrition is performed using zirconia balls of 800 µm diameter. After 3 h, the mixture is separated from the balls with a 200 µm sieve, dried and calcined 5h at 1100°C until perovskite phase formation. Then, the powder is once again attrition-milled in ethanol. Each 15 minutes during the attrition milling, a granulometry analysis is done using a laser granulometer (Horiba LA950), in order to obtain the desired monomodal grain size distribution with a mean diameter close to 1 µm.

$LSFCo_{6482}$ powder used for the electrophoretic suspension is produced by citrate route [Xu 2004]. The stoichiometric amount of metal nitrate ($Sr(NO_3)_2$ (≥ 99.0 %, Sigma-Aldrich), $Fe(NO_3)_3.9H_2O$ (98+ %, Alfa Aesar), $La(NO_3)_3.6H_2O$ (99.9 %, Alfa Aesar) and $Co(NO_3)_2.6H_2O$ (98.0-102.0 %, Alfa Aesar)) are mixed and dissolved in deionized water. Then, solid citric acid (99+% Alfa Aesar) is introduced into the mixed solution and under magnetic stirring. The molar ratio of citric acid to metal nitrate is fixed at [CA]/[M]=1.5. After 30 minutes, a 28% ammonia solution is introduced in the mixed solution in order to reach a pH around 9.5 (the precipitation point is exceeded). The solution is heated at 120 °C until a gel is obtained which is then heated at 320 °C to provoke the auto-combustion. The powder obtained after auto-combustion is calcined at 1100 °C for 4 h to have an as pure as possible perovskite phase. The powder produced is characterized by Scanning Electron Microscopy (SEM, Cambridge instrument) and by laser granulometer (Horiba LA950). The mean grain size (Diffusion Laser Scattering, DLS) and the density of powders (gas pycnometer, Accupyc II 1340, Micormeritics) are reported in Table 1. .

For each powder, the formation of a perovskite phase is confirmed by X-ray diffraction (Siemens D5000, Cu-$K_{\alpha 1}$) and chemical composition is verified by inductively coupled plasma atomic emission spectrometer.

2.2 Preparation of the substrate by tape casting

Dense membranes are elaborated by tape casting [Chartier 1994]. An $LSFCo_{6482}$ slurry is prepared from the powder obtained by solid state synthesis, an organic solvent, a dispersant (phosphate ester), a binder and a plasticizer. Powder, organic solvent and dispersant are first ball-milled for 1 h, then the binder and the plasticizer are added to obtain a slurry with an adapted rheology for tape casting. A green tape of 150 µm thickness is tape-cast, dried and punched into disks of 30 mm diameter. Then, those disks are stacked (to obtain 1 mm thick membrane after sintering) and thermo-laminated under 50MPa at 70 °C. The green membranes are debinded and

sintered to 1350 °C at a rate of 5 °C/min with a dwell of 4 h to obtain a relative density higher than 95%. The relative density of the membrane is measured using Archimedes method.

2.3 Electrophoretic coating procedure

The suspension for electrophoretic deposition is prepared by adding to the $LSFCo_{6482}$ powder to the ethanol solvent and 1.5 wt.% of dispersant (phosphate ester). The $LSFCo_{6482}$ powder concentration is 5 wt.% in slurry. The suspension is ball-milled at 260 rpm for 1 h to homogenize the suspension. Then, 2 wt.% of binder (Degalan 51/07, Degussa, Germany) is added to the suspension and ball-milled again 12 h at 130 rpm. The addition of binder improves the cohesion of the green electrophoretic coating after drying.

The electrophoretic cell presented **Figure 1** consists in an anodic substrate centered between two parallel copper cathodic electrode plates (50.1*41.4*0.4 mm^3). The electrodes are movable, they can be spaced with distances from 0.5 to 5 cm. For this experiment, the distance is set at 3 cm and the submerged surface of the electrodes is 18.5 cm^2. A very slow stirring by magnetic stirrer prevents from the sedimentation of the suspension. A generator allows to adjust the voltage from 0 to 84 V between the electrodes. After coating, each membrane is taken out of the suspension and the deposit is dried at room temperature at least during 4 h. Then, the membrane with the dried coating is heated to 1150 °C for 2 h at a rate of 1 °C/min to remove all organic components and to further consolidate the porous coating. The remaining porosity in the coating is favorable to the diffusion of the gas through the thickness of the coating, which makes it possible oxygen adsorption on each perovskite particle on the pore surface in the thickness of coating.

Powders, substrate and coatings are observed by SEM to evaluate the morphology and the size of the grains but also the uniformity and the thickness of the coating.

2.4 Electrochemical characterizations

2.5.1. Oxygen semi-permeation measurements of membranes

Electrochemical performances i.e. oxygen semi-permeation flux and oxygen activities at the membrane surfaces are measured using a specific setup reported in **Figure 2** and described in previous work [Vivet 2011]. The membrane sealed between two alumina tubes by gold rings separates three chambers. In the first chamber, recombined air is injected (100 mL/min, oxygen-rich atmosphere), in the second chamber, argon is injected (200 mL/min, oxygen-lean atmosphere). The two different gas flows generate an oxygen partial pressure gradient through the membrane which is the driving force for oxygen diffusion through the membrane. The last chamber

is used to avoid transversal leak. An argon flux is also injected in this chamber. The tightness between the chambers are checked at high temperature (900°C) before the measurements of oxygen semi-permeation. Measurements are performed from 970 °C to 600°C with an interval of 10 °C between each measure.

2.5.2 Oxygen semi-permeation measurement

The oxygen flux through the membrane is calculated using the following equation:

$$J_{O_2} = \frac{D_{Ar}}{V_{m\,(Ar)}} \frac{(P_{2out} - P_{2in})}{S} \quad \textbf{(Eq. 1)}$$

Where J_{O_2} is the oxygen flux through the membrane in mol.m^{-2}.s^{-1}, D_{Ar} the Argon flow in l.s^{-1}, $V_{m\,(Ar)}$ the molar volume of argon in l.mol^{-1}, S the apparent membrane surface in m².

P_{2out} and P_{2in} are the oxygen partial pressure in the outlet argon flux and the oxygen partial pressure in the argon flux (in atm), respectively. They are evaluated from the electromotive force $E_{(g)\,2out}$, thanks to YSZ-oxygen sensors, following the Nernst law:

$$E_{(g)\,2out} = \frac{RT}{4F} ln \frac{P_{2out}}{P_{O_2}} \quad \textbf{(Eq. 2)}$$

Where R is the universal gas constant, F the Faraday constant and T the temperature and P_{O2} is the oxygen partial pressure in the air (= 0.21 atm).

3 Results and discussion

3.1 Characterization of the perovskite powders and of the dense membrane

Table 1 and **Figure 3 A and B** show the main characteristics of the $LSFG_{5573}$ powder produced by solid state reaction and $LSFCo_{6482}$ powder produced by citrate route before milling. The mean grain size of $LSFG_{5573}$ powder is close to 1 micron which is adapted to tape casting process (Table 1). The mean grain size of $LSFCo_{6482}$ powder (i.e. 0.4 µm) is smaller than that of $LSFG_{5573}$ powder. The low grain size of $LSFCo_{6482}$ powder is favorable to a high exchange surface of electrophoretic coating to improve the kinetics of oxygen surface exchange of the membrane. Powder stoichiometry checked by ICP-AES analysis (**Table 2)** show a chemical composition of $LSFG_{5573}$ and $LSFCo_{6482}$ powders close to the chemical compositions expected, Table 2.

Table 1. *Characterization of perovskite powders*

	Synthesized route	Mean grain size (µm)	Powder density ($g.cm^{-3}$)
$LSFG_{5573}$	Solid state reaction	0.9	5.94
$LSFCo_{6482}$	Citrate route	0.4	6.00

Table 2. *Chemical elementary analysis of $LSFG_{5573}$ and $LSFCo_{6482}$ powders obtained by Induced Coupling Plasma (ICP)*

Elements	**stoichiometry measured by ICP**	**stoichiometry desired**
	$LSFG_{5573}$ (solid state reaction)	
La	0.52	0.5
Sr	0.48	0.5
Fe	0.71	0.7
Ga	0.29	0.3
	$LSFCo_{6482}$ (citrate route)	
La	0.59	0.6
Sr	0.41	0.4
Fe	0.78	0.8
Co	0.22	0.2

Figure 3 C1 and C2 shows SEM micrographs of the surface and fracture section of $LSFG_{5573}$ dense membrane. The bulk mean grain size is around 2 µm and a density of 95%. The grain size has a significant impact on the electrochemical performances. Indeed, recent work shows that large grain size (up to 1-2 microns) is usually favorable to ionic conduction through the membrane bulk [Reichmann 2016].

Figure 4 shows the X-ray diffraction patterns of $LSFCo_{6482}$ powders produced by citrate route, $LSFG_{5573}$ powder produced by solid state reaction and $LSFG_{5573}$ sintered membrane. The $LSFCo_{6482}$ powder has a well-defined perovskite phase without apparent secondary phase. The $LSFG_{5573}$ powder synthesized by solid state reaction has the expected perovskite phase but also two secondary phases determined has La_2O_3 and $SrLaGa_3O_7$. After the shaping of the powder by tape casting and the sintering of the obtained pellets, the La_2O_3-secondary phase disappears but the $SrLaGa_3O_7$-secondary phase still remain. This secondary phase has a low impact the oxygen diffusion coefficient, but it could have a large impact on the oxygen surface exchange kinetics. The impact of secondary phases on oxygen transport mechanism through the $La_{1-x}Sr_xFe_{1-y}Ga_xO_{3-\delta}$ perovskite membrane the will be discussed in a further study.

3.2 Impact of the electrophoretic parameters on the coating

3.2.1 Impact of the applied voltage on the coating thickness

Figure 5 and 6 shows the influence of the applied voltage on the coating thickness for an electrophoretic coating time of 120 s. From 0 to 5 V, a very few particles are scattered (patchy) on the membrane surface, and the coating thickness is less than 10 µm. From 5 to 60 V, there is a linear relation between the coating thickness and the voltage. Above 60 V, the growth rate of the coating highly decreases with the voltage. Besides, the thickness homogeneity of the deposits decreases when the applied voltage increases in agreement with the results reported by Besra et al. [Besra 2007]. The homogeneity of the coating is likely linked to the migration speed of particle in suspension. When the applied electrical field is high, the migration speed of particles is high in the suspension, that is likely not favorable to obtain a well-packed layer. However, if the voltage is low (below 2-3 V), there is not electrophoretic coating because the electrostatic forces on the ceramic particles are too low in comparison to the forces linked to mechanical agitation (or Brownien agitation) in the suspension during the electrophoretic coating.

Then, the voltage will be fixed to 20 V in the following sections of this study, which correspond to a good compromise between a compact layer and suitable migration rate of ceramic particles in the suspension.

3.2.2 Impact of the coating time on the deposit thickness

Figure 7 shows the evolution of the coating thickness in relation with the electrophoretic coating time. The coating thickness linearly increases with the time from 30 to 300 s. Above 300 s, the depletion of perovskite particles in suspension leads to a significant slowdown in the growth of the electrophoretic coating [Besra 2007]. The maximum thickness of electrophoretic coating obtained in this study cannot be exceed 220 µm, because the growth of coating is too low above 200 µm due to the depletion of perovskite particles in the suspension.

3.3 Electrochemical performances

Electrochemical performances were studied for a dense $LSFG_{5573}$ membrane without coating, and three dense $LSFG_{5573}$ membranes coated with different thickness of $LSFCo_{6482}$ porous layer on both surfaces of $LSFG_{5573}$ dense membrane.

Figure 8 A shows the evolution of the oxygen semi-permeation flux versus the temperature for different thicknesses of the porous layer deposited on the $LSFG_{5573}$ dense membrane surfaces. **Figure 8 B** shows the oxygen semi-permeation flux at 900°C versus the thickness of the porous layer. The oxygen flux increases with

the thickness of the coating. The highest oxygen flux (2.6×10^{-3} mol.m^{-1}.s^{-1} at 900 °C) is obtained for a membrane with a porous layer of 115 µm in thickness. Moreover, the oxygen flux shows a quasi-linear evolution with the thickness of the coating. The previous work shows clearly that the oxygen flux of dense $LSFG_{5573}$ membranes is mainly governed by the oxygen surface exchange [Xu 1999]. Then, the surface developed by the open porosity in $LSFCo_{6482}$ coating is likely proportional to the thickness of the coating. Then, it could be interesting to study larger thickness of the porous coating to determine the optimum. Unfortunately, the electrophoretic coating method described in this work does not allow to excess 100-120 microns in thickness after sintering due to the delamination of the electrophoretic coating during the calcination step.

Arrhenius plot and activation energies of the four different membranes are reported **Figure 9** and **Table 3,** respectively. The activation energy (Ea) decreases when the thickness of the electrophoretic coating increases. This trend is linked to the evolution of the limiting step of the oxygen transport through the membrane when the thickness of porous coating increases. Indeed, a recent work shows that the oxygen flux through a dense LSG_{5573} membrane is mainly governed by the kinetics of oxygen surface exchanges [Xu 1999]. Then, the kinetic of oxygen surface exchanges increases with the coating thickness or the surface developed by the porosity of electrophoretic coating. An increasing of the coating thickness leads to an evolution of the limiting step and then the apparent energy activation of oxygen flux through the membrane. This suggests that the oxygen flux is mainly governed by bulk diffusion through the membrane when the thickness of porous coating is large (up to 100 microns in this work).

Besides, a previous work [Vivet 2014] reported an activation energy of oxygen flux governed by oxygen diffusion in the bulk through $La_{0.6}Sr_{0.4}Fe_{0.6}Ga_{0.4}O_{3-\delta}$ ($LSFGa_{6464}$) dense membrane close to 70 kJ mol^{-1}, suggesting that $LSFGa_{5573}$ material has similar oxygen transport properties than $LSFGa_{6464}$ material. Also, the energy activation of the oxygen flux through $LSFGa_{5573}$ dense membrane with a porous coating of 115 µm in thickness is close to 60 kJ.mol^{-1}, and corresponds to the energy activation of the oxygen flux through $LSFGa_{6464}$ membrane when the oxygen flux is governed by oxygen diffusion the bulk (i.e. close to 70 kJ. mol^{-1}).

Table 3. *Activation energy calculated from Arrhenius plot* of oxygen flux through $LSFG_{5573}$ dense membrane without and with porous coating.

	Temperature (°C)	***Ea (kJ.mol^{-1})***	***Temperature (°C)***	***Ea (kJ.mol^{-1})***
0 µm	*970 to 820*	*120*	*820 to 640*	*155*
5 µm	*965 to 835*	*130*	*835 to 695*	*160*
75 µm	*966 to 790*	*100*	*790 to 620*	*129*
115 µm	*960 to 800*	*51*	*800 to 620*	*60*

Table 3 shows that the evolution of activation energy in relation with the range of temperature. The activation energy increases at lower temperature. The first assumption is that the evolution of energy activation is linked to the evolution of the predominant limiting step with the temperature. Indeed, the oxygen flux through the membrane is mainly governed by surface exchange at low temperature and by oxygen bulk diffusion at high temperature (usually up to 1000°C), as previously reported [Vivet 2011].

The coating thickness does not have the same impact on the kinetic coefficient at the oxygen-rich side and at the oxygen-poor side because the oxygen concentration of the gases and consequently the migration kinetic of the oxygen through the coatings are very different between the two faces of the ceramic membrane Indeed, the oxygen migration flux in the gaseous phase through the coating is proportional to its concentration as expressed by the Fick law (Eq. 8):

$$J_{O_2} = D_{O_2} \frac{\Delta P_{O2}}{e} \qquad \text{(Eq. 8)}$$

With e the thickness of the porous coating, D_{O2} the oxygen permeation coefficient (depending on the porous coating) and ΔP_{O2} the gradient of oxygen partial pressure.

In opposite, the oxygen migration flux in the bulk of the dense membrane is proportional to the gradient of $\ln P_{O2}$ (and not to P_{O2}), which is expressed by the Wagner law (Eq. 9):

$$J_{O_2} = \frac{C_O D_O}{4} \frac{\Delta \ln P_{O2}}{L} \qquad \text{(Eq. 9)}$$

With L the thickness of the dense membrane, C_O the oxygen concentration in the material of the dense membrane D_O the oxygen diffusion coefficient. $\Delta \ln P_{O2}$ corresponds to the gradient of oxygen chemical potential.

The Fick law assumes that the gradient of oxygen partial pressure through the porous coating on the rich and poor-oxygen sides are similar, because the oxygen flux is constant through the membrane and the thickness of the porous coating is similar on both side of the membrane (see eq.8). However, the similar gradient of oxygen partial pressure has not the same impact on the driving force of oxygen flux or gradient of oxygen chemical potential through the membrane. Indeed, the oxygen flux is proportional to the gradient of oxygen chemical potential through the dense membrane, as reported previously by the Wagner law in eq. 9.

For instance, the oxygen partial pressures on the poor and rich-oxygen sides are 10^{-3} and 0.21 atm. at 900°C, respectively. The gradients of oxygen partial pressure through both porous coatings are similar, estimated here to $\Delta P = 5.\ 10^{-4}$ atm. This leads to a very low gradient of oxygen chemical potential through porous coating at rich-oxygen side ($\Delta\mu_{O2\ (rich)} = RT \ln 0.21/(0.21-\Delta P)) = 23\ J.mol^{-1}$) and large gradient of oxygen chemical potential through the porous coating at poor-oxygen side ($\Delta\mu_{O2\ (poor)} = RT \ln (10^{-3}-\Delta P)/(10^{-3}) = 3.9\ 10^{3}\ J.mol^{-1} >> \Delta\mu_{O2\ (rich)}$), as reported on figure 10. It is then possible to conclude that the oxygen migration step through the porous coating at the poor-oxygen side can limit the oxygen flux through the dense membrane, when the porous coating is very thick. The higher coefficient of oxygen surface exchanges is obtained for the membrane with the thicker porous layer in the thickness range tested (i.e. up to 115 µm) but an optimum thickness will likely exist.

4 Conclusions

A dense $LSFG_{5573}$ membrane has been coated by electrophoretic coating method, with $LSFCo_{6482}$ particles of 0.45 µm diameter. This selection of materials was chosen wisely because it combines high oxygen diffusion coefficient for $LSFG_{5573}$ material used as the dense membrane and high kinetics of oxygen surface exchanges with $LSFCo_{6482}$ materials used as porous coating. This association of the two materials leads to a very high oxygen semi-permeation, i.e. 2.6×10^{-3} $mol.m^{-1}.s^{-1}$ at 900 °C, which corresponds to the high oxygen flux performances in the literature. However, these oxygen flux performances are lower than the oxygen fluxes obtained with $Ba_{1-x}Sr_xFe_{1-y}Co_yO_{3-\delta}$ perovskite membranes, i.e. from 1 to 20×10^{-3} $mol.m^{-2}.s^{-1}$ at 900 °C, which are among the best performances ever reported in the literature for membrane materials [Ge 2008, Ge 2009].

However, $La_{0.5}Sr_{0.5}Fe_{0.7}Ga_{0.3}O_{3-\delta}$ perovskite membranes have a better chemical stability and mechanical properties than $Ba_{1-x}Sr_xFe_{1-y}Co_yO_{3-\delta}$ perovskite membranes in working conditions.

The impact of the electrophoretic voltage on the migration rate of particles has been established. However, when the coating thickness is large (up to 100 microns), the migration rate of particle decreases significantly. Then, the maximum coating thickness obtained by electrophoretic coating is limited to 100-120 microns due to the delamination of coating during the calcination step.

The higher oxygen flux is obtained with the membrane coated with the thickest coating possible to obtain, i.e. 115 µm. This suggest that the oxygen flux is mainly governed by the oxygen surface exchange at the membrane, but not by the oxygen bulk diffusion through the dense membrane.

Finally, this study shows that the electrophoretic coating is interesting method to obtain very homogenous porous coating from 2-5 µm to 115 µm thickness. The microstructure of electrophoretic coating is adapted to obtain a perovskite coating with high electrochemical performances. This should be particularly interesting for the elaboration of cathode materials for SOFC application.

Acknowledgements

The authors wish to express their gratitude to Air Liquide Company for financial and technical support and the ADEME (French Environment and Energy Management Agency) for financial support of this study.

References

Besra L., Liu M., 2007, A review on fundamentals and applications of electrophoretic deposition (EPD), Progress in Materials Science, 52, 1-61.

Boccaccini A.R., Zhitomirsky I., 2002, Application of electrophoretic and electrolytic deposition techniques in ceramics processing, Current Opinion on Solid state and Materials Science, 6, 251-260.

Chartier T., 1994, Tape casting, The Encyclopedia of Advanced Materials, vol. 4, Pergamon, Cambridge 1763-1767.

Etchegoyen G., Chartier T., Del Gallo P., 2006, An architectural approach to the oxygen permeability of a $La_{0.6}Sr_{0.4}Fe_{0.9}Ga_{0.1}O_{3-\delta}$ perovskite membrane, Journal of European Ceramic Society, 26, 13, 2807-2815.

Ge L., Ran R., Zhang K., Liu S., Shao Z., 2008, Oxygen selective membranes based on B-site cation-deficient (Ba0.5Sr0.5)(Co0.8Fe0.2)yO3-8 perovskite with improved operational stability, J. Membr. Sci. 318, 182.

Ge L., Shao Z., Zhang K., Ran R., Diniz da Costa J.C., Liu S., 2009, Evaluation of Mixed-Conducting Lanthanum-Strontium-Cobaltite Ceramic Membrane for Oxygen Separation, AIChE Journal 55, 2603.

Geffroy P.-M., Fouletier J., Richet N., Chartier T., 2013, Rational selection of membrane materials of MIEC materials in energy production precesses, Chemical Engineering Science, 87, 408-433.

Geffroy P.-M., Reichmann M., Kilmann L., Jouin J., Richet N., Chartier T., 2015, Identification of the rate-determining step in oxygen transport through La(1-x)SrxFe(1-y)GayO3-δ perovskite membranes, Journal of Membrane Science, 476, 340-347.

Geffroy P.-M., Blond E., Richet N., Chartier T., 2017, Understanding and identifying the oxygen transport mechanisms through mixed-conductor membranes, Chemical Engineering Sciences, 162, 245-261**.**

Guironnet L., Geffroy P.-M., Richet N., Chartier T., 2016, Improvement of oxygen flux through perovskite membranes using a coating of ultra-divided particles, Chemical Engineering science, 156, 128-135.

Hamaker H.C., 1940, Formation of a deposit by electrophoresis, Trans. Faraday Soc., 35, 279-287.

Hayamizu Y., Kato M., Takamura H., 2014, Effects of surface modification on the oxygen permeation of $Ba_{0.5}Sr_{0.5}Co_{0.8}Fe_{0.2}O_{3-\delta}$, J. Membr. Sci., 462, 147-152.

Heavens N., *Electrophoretic deposition as a processing route for ceramics, Advances ceramic processing and technology*, vol 1, 1990, 255-83 [chap 7]

Majhi S.M., Behura S.K.,' Bhattacharjee S., Singh B.P., Chongdar T.K.,' Gokhale N.M., Besra L., 2011, Anode supported solid oxide fuel cells (SOFC) by electrophoretic deposition, International Journal of Hydrogen Energy, 36, 22, (2011) 14930-14935.

Powell J., Petring D., Kumar R.V., Al-Mashikhi S.O., Kaplan A.F.H., Voisey, 2019, Laser-oxygen of mild steel: the thermodynamics of the oxidation reaction, Journal of Physics D: Applied Physics, 42-1.

Reichmann M., Geffroy P.-M., Richet N., Chartier T., 2016, Impact of microstructure on oxygen semi-permeation performance of perovskite membranes: understanding of oxygen transport mechanisms, J. Power Sources 324, 774–779.

Schulz M., Pippardt U., Kiesel L., Ritter K., Kriegel R., 2010, Oxygen permeation of various archetypes of oxygen membranes based on BSCF, AlChE Journal, 58, 3195-3202.

Sunsaro J., Baumann S., Serra J.M., Meulenberg W.A., Liu S., Lin Y.S., Diniz da Costa J.C., 2008, Mixed ionic-electronic conducting (MIEC) ceramic-based membranes for oxygen separation, Journal of Membrane Science, 320, 13-41.

Tan X., Wang Z., Meng B., Meng X., Li K., 2010, Pilot-scale production of oxygen from air using perovskite hollow fibre membranes, Journal of Membrane Science, 352, 189-196.

Vivet A., Geffroy P.-M., Coudert V., Fouletier J., Chartier T., Richet N., 2011, Influence of glass and gold sealants materials on oxygen permeation performances in $La_{0.8}Sr_{0.2}Fe_{0.7}Ga_{0.3}O_{3-\delta}$ perovskite membranes, Journal of Membrane Science, 366 (1-2), 132-138.

Vivet A., P.-M. Geffroy P.-M., Thune E., Bonhomme C., Rossignol F., Richet N., Chartier T., New route for high oxygen semi-permeation through surface-modified dense $La_{1-x}Sr_xFe_{1-y}Ga_yO_{3-\delta}$ perovskite membranes, Journal of Membrane Science, 454 (2014) 97-108.

Xu S.J., Thomson W.J., 1999, Oxygen permeation rates through ion-conducting perovskite membrane, Chem. Eng. Sci., 54, 3839-3850.

Xu Q., Huang D., Chen W., Lee J., Wang H., Yuan R., 2004, Citrate method synthesis, characterization and mixed electronic-ionic conduction properties of La0.6Sr0.4Co0.8Fe0.2O3-d perovskite-type complex oxides, Scripta Materialia, 50, 165-170.

Zhang C., Xu Z., Chang X., Zhang Z., Jin W., *Preparation and characterization of mixed-conducting thin tubular membrane*, Journal of Membrane Science, 299 (2007) 261-267.

Zhitomirsky I., A. Petric A., 2000, Electrophoretic deposition of ceramic materials for fuel cell applications Journal of the European Ceramic Society, 20, 2055–2061.

Figure captions

Figure 1. Electrophoretic coating cell

Figure 2. Oxygen semi-permeation setup

Figure 3. Micrographs of A) $LSFG_{5573}$ perovskite powders (solid state reaction) and B) $LSFCo_{6482}$ perovskite powders (citrate route), of the $LSFG_{5573}$ dense membrane C1) surface and C2) cross section.

Figure 4. XRD patterns of $LSFCo_{6482}$ citrate powder, $LSFG_{5573}$ dense membrane and $LSFG_{5573}$ solid state reaction powder

Figure 5. Micrographs of the coating obtained by electrophoretic coating during 120s with a voltage of A) 5V, B) 40V and C) 80V

Figure 6. Impact of the applied voltage on the thickness and on the homogeneity of coating for an electrophoretic coating time of 120s

Figure 7. Impact of the coating time on the coating thickness, for an applied voltage of 20V

Figure 8. Evolution of the oxygen semi-permeation A) as function of the temperature and B) as function of the thickness of the porous layer at 900°C

Figure 9. Arrhenius plot of oxygen flux trough $LSFG_{5573}$ dense membrane without and with porous coating obtained by electrophoretic method.

Figure 10. Hypothesis on the profile of oxygen chemical potential ($RT\ lnP_{02}$) through the dense membrane with porous coating on poor and rich oxygen side.

Table captions

Table 1. Characterization of perovskite powders

Table 2. Chemical elementary analysis of $LSFG_{5573}$ and $LSFCo_{6482}$ powders obtained by Induced Coupling Plasma (ICP)

Table 3. Activation energy calculated from Arrhenius plot of oxygen flux trough $LSFG_{5573}$ dense membrane without and with porous coating

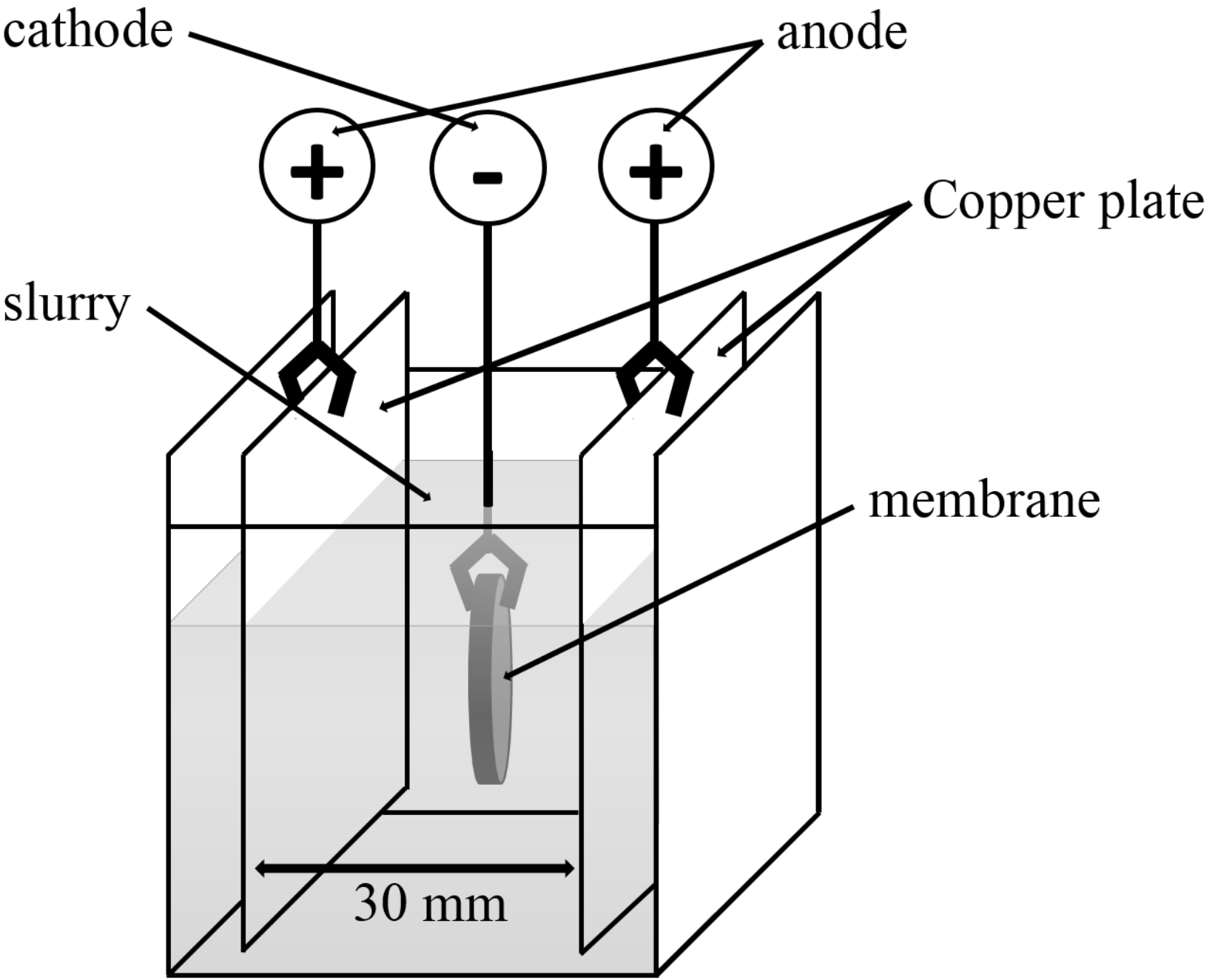
cathode
anode
+
-
+
Copper plate
slurry
membrane
30 mm

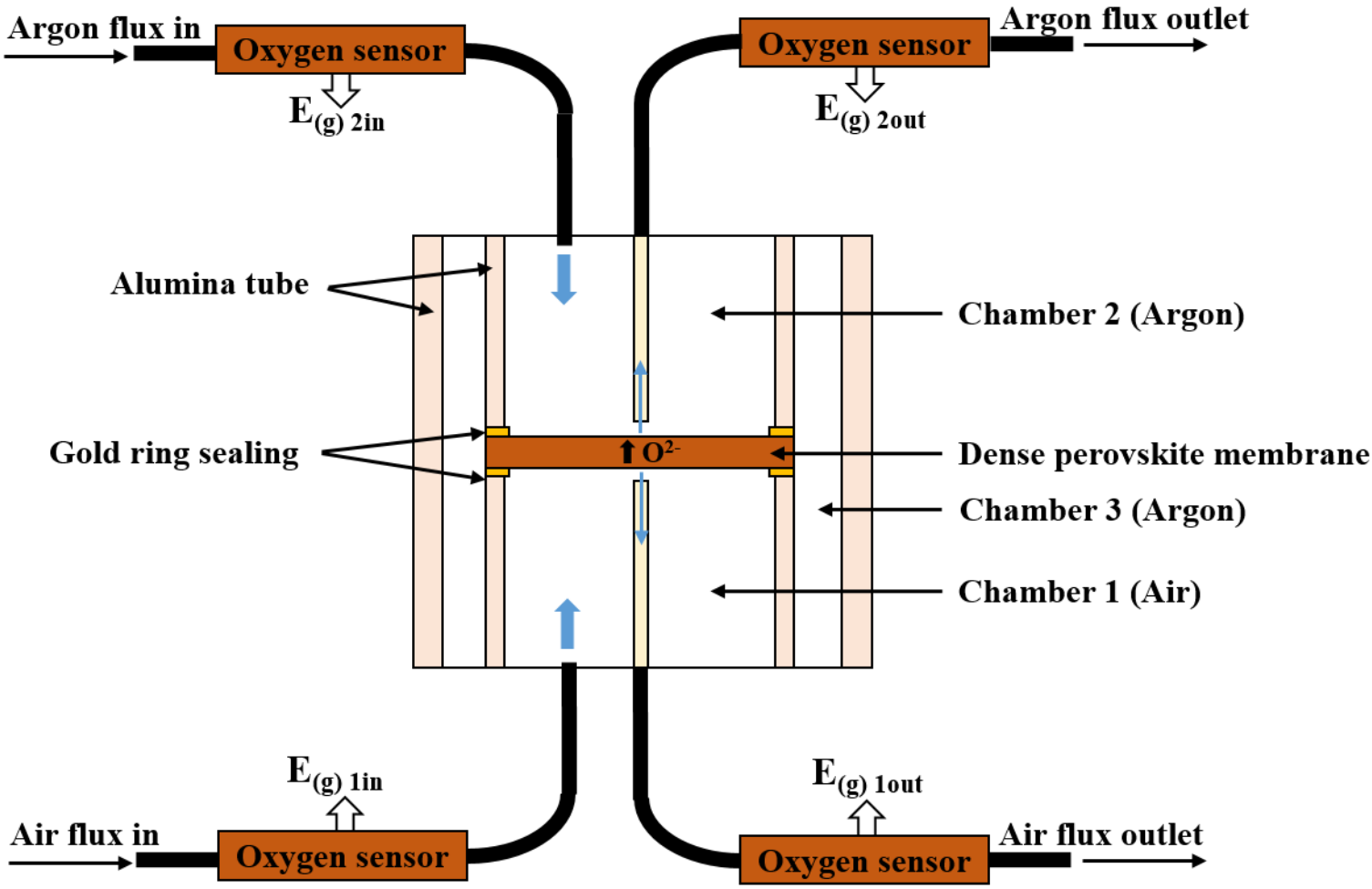
Argon flux in
Oxygen sensor
$E_{(g)\ 2in}$
Oxygen sensor
Argon flux outlet
$E_{(g)\ 2out}$
Alumina tube
Chamber 2 (Argon)
Gold ring sealing
O^{2-}
Dense perovskite membrane
Chamber 3 (Argon)
Chamber 1 (Air)
$E_{(g)\ 1in}$
$E_{(g)\ 1out}$
Air flux in
Oxygen sensor
Oxygen sensor
Air flux outlet

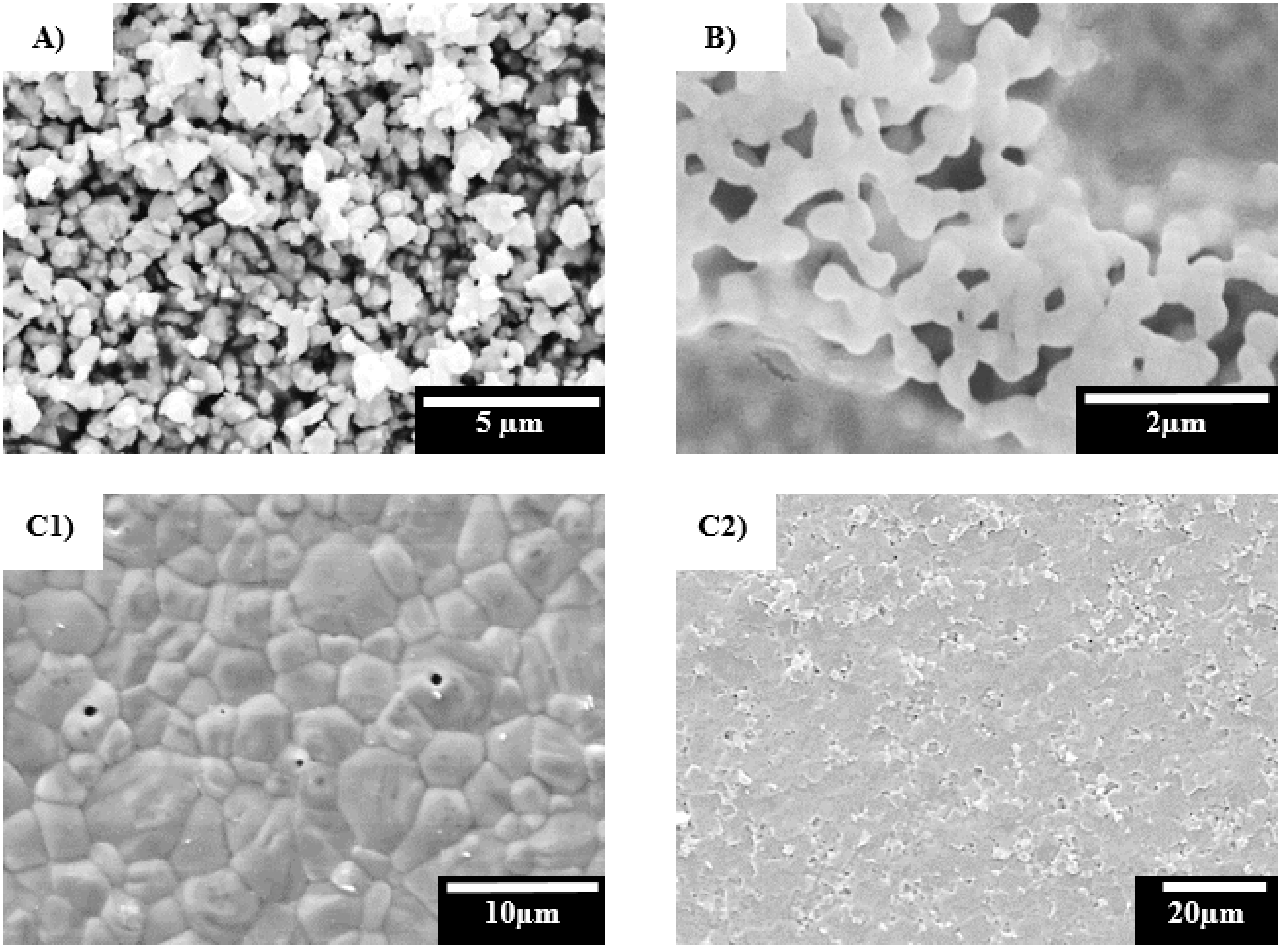
A)
5 µm
B)
2µm
C1)
10µm
C2)
20µm

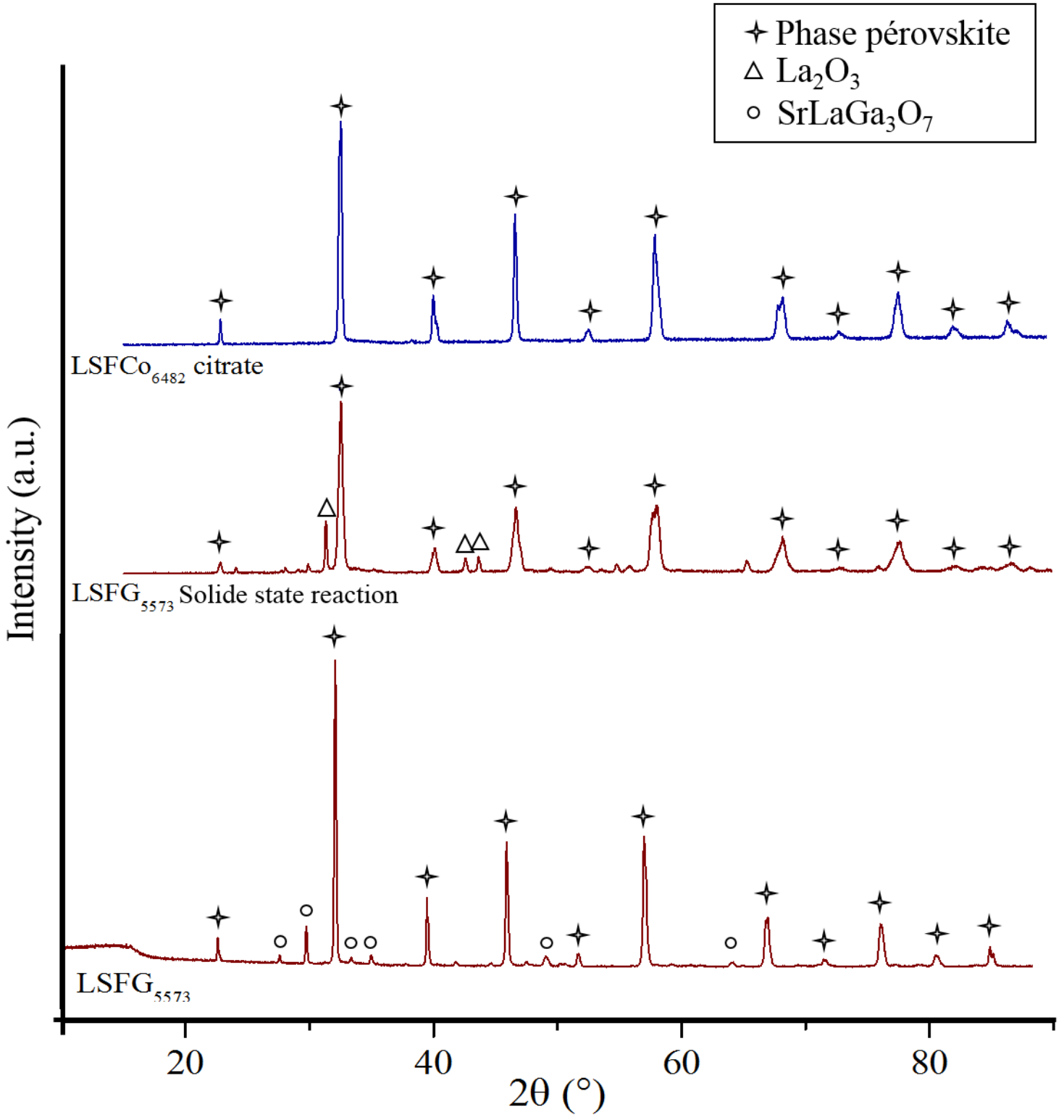
Phase pérovskite
La2O3
SrLaGa3O7
LSFCo6482 citrate
LSFG5573 Solide state reaction
LSFG5573
Intensity (a.u.)
20
40
60
80
2θ (°)

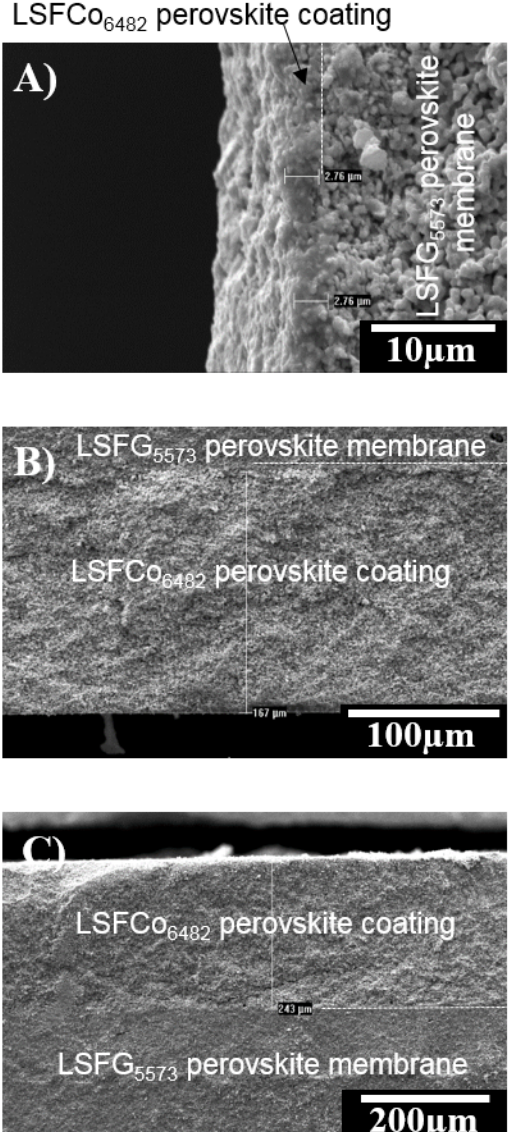
LSFCo6482 perovskite coating
A)
2.76 µm
2.76 µm
LSFG5573 perovskite membrane
10µm
B)
LSFG5573 perovskite membrane
LSFCo6482 perovskite coating
167 µm
100µm
C)
LSFCo6482 perovskite coating
243 µm
LSFG5573 perovskite membrane
200µm

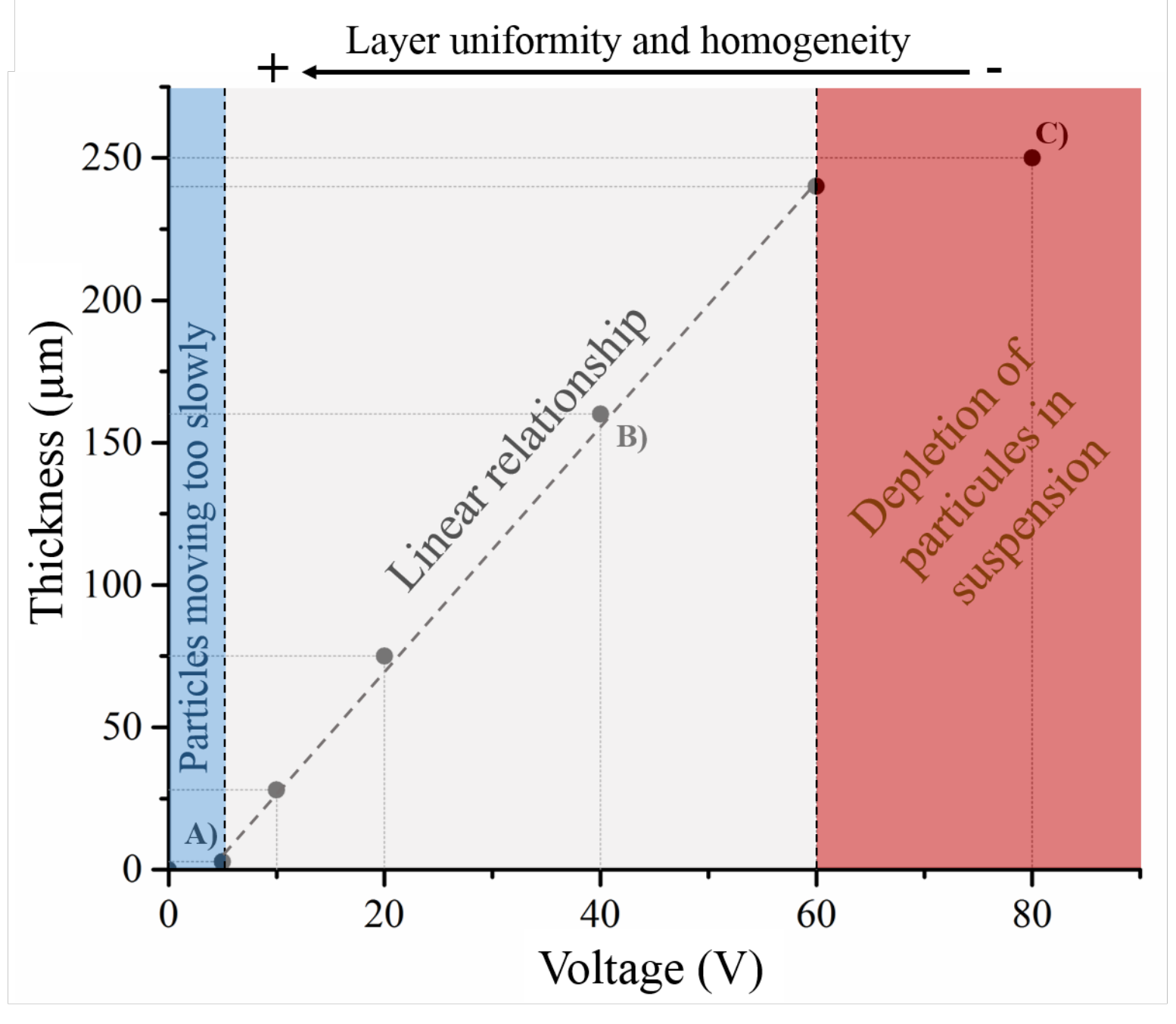
Layer uniformity and homogeneity
+
-
Thickness (µm)
0
50
100
150
200
250
0
20
40
60
80
Voltage (V)
Particles moving too slowly
Linear relationship
Depletion of particules in suspension
A)
B)
C)

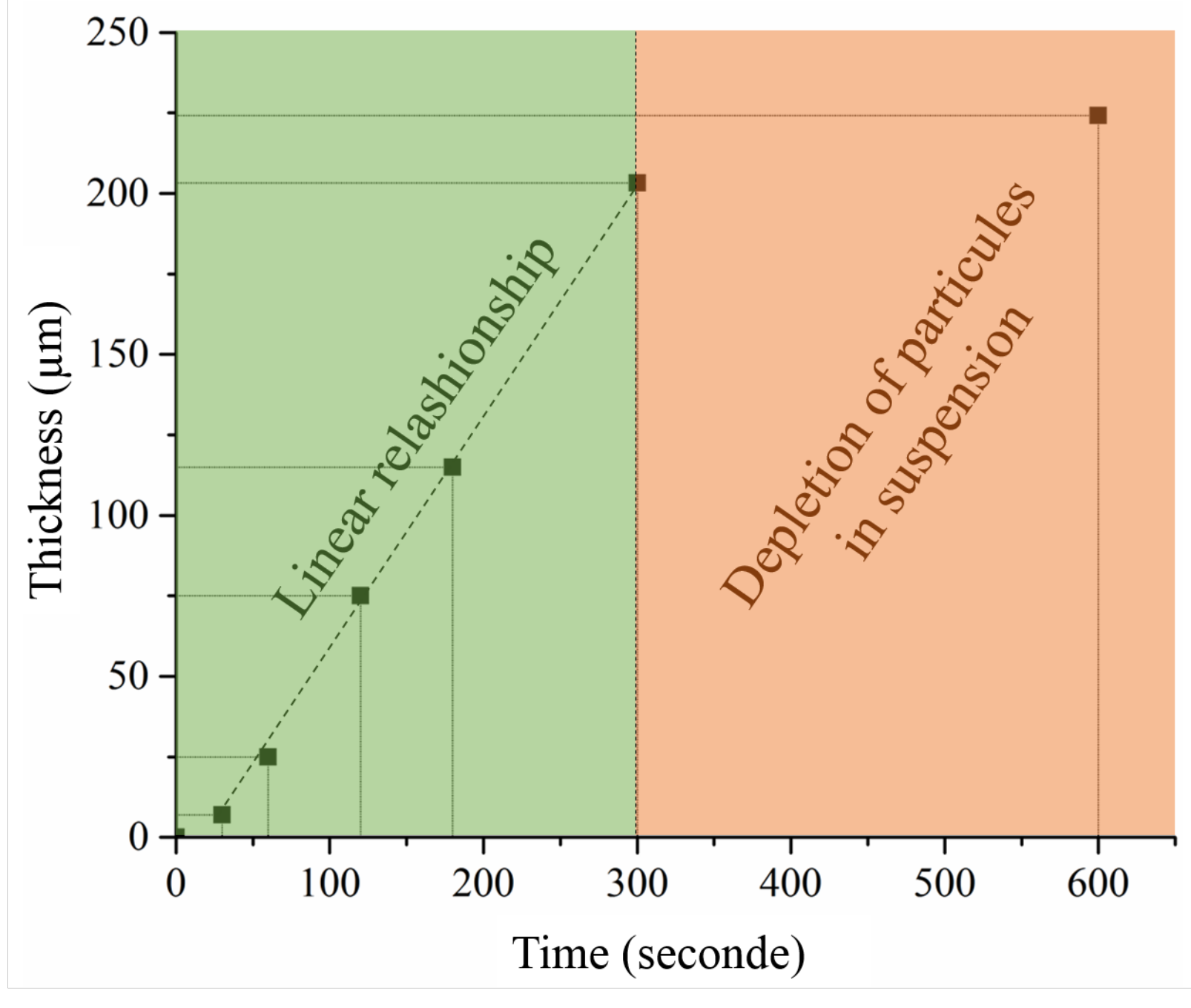
Thickness (µm)
250
200
150
100
50
0
0
100
200
300
400
500
600
Time (seconde)
Linear relashionship
Depletion of particules
in suspension

A)

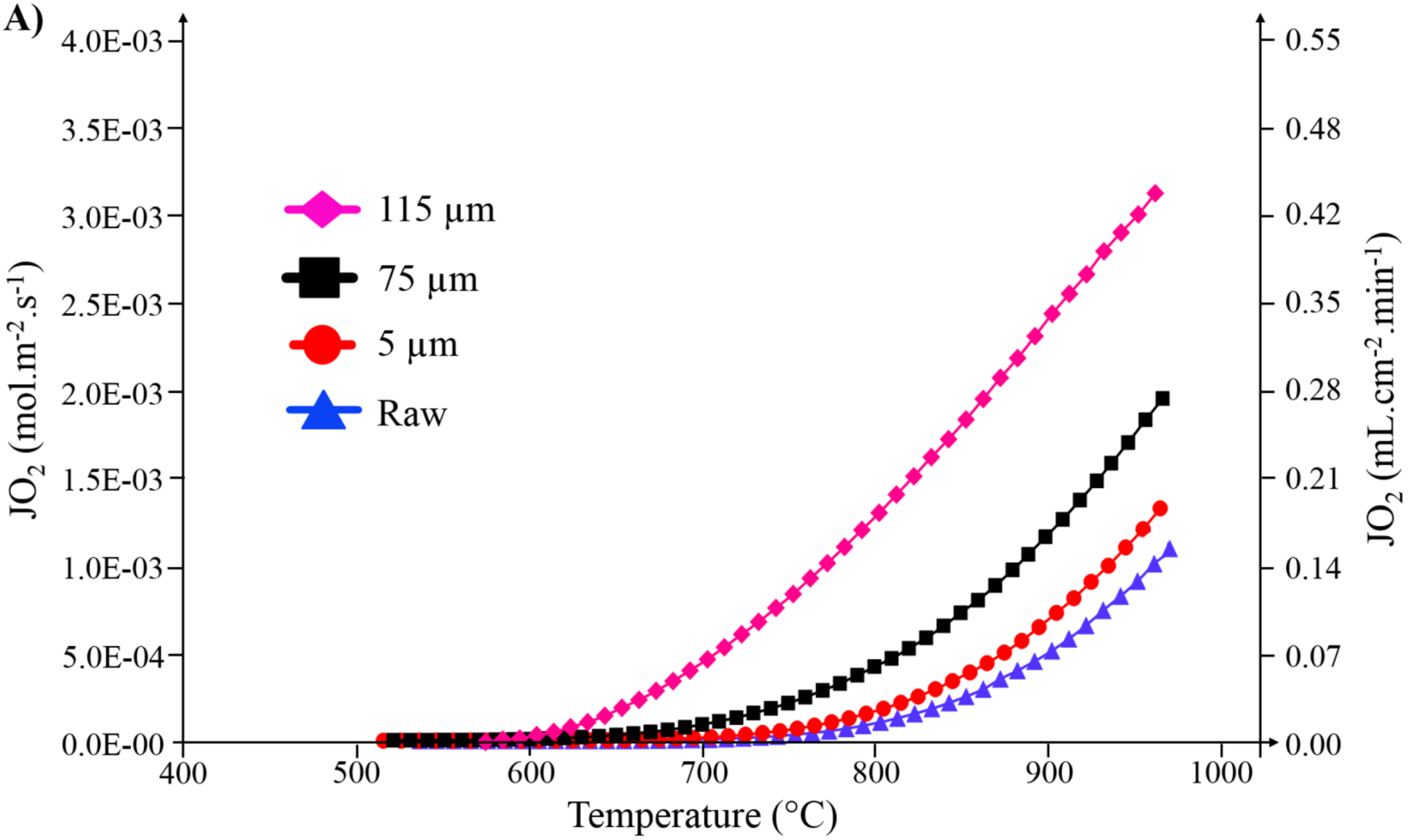
4.0E-03
3.5E-03
3.0E-03
2.5E-03
2.0E-03
1.5E-03
1.0E-03
5.0E-04
0.0E-00
JO2 (mol.m-2.s-1)
0.55
0.48
0.42
0.35
0.28
0.21
0.14
0.07
0.00
JO2 (mL.cm-2.min-1)
115 µm
75 µm
5 µm
Raw
400
500
600
700
800
900
1000
Temperature (°C)

B)

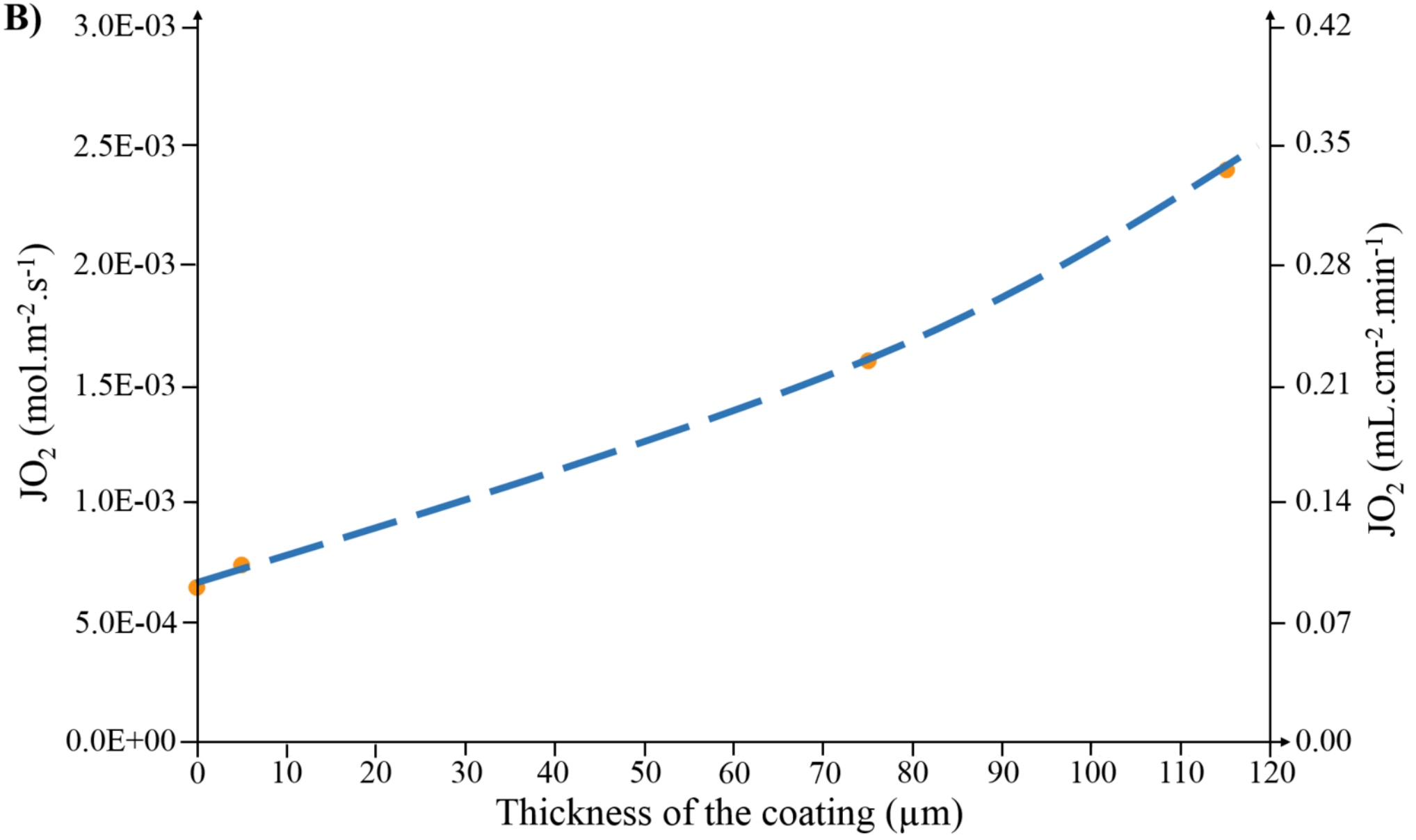
3.0E-03
2.5E-03
2.0E-03
1.5E-03
1.0E-03
5.0E-04
0.0E+00
JO2 (mol.m-2.s-1)
0.42
0.35
0.28
0.21
0.14
0.07
0.00
JO2 (mL.cm-2.min-1)
0
10
20
30
40
50
60
70
80
90
100
110
120
Thickness of the coating (µm)

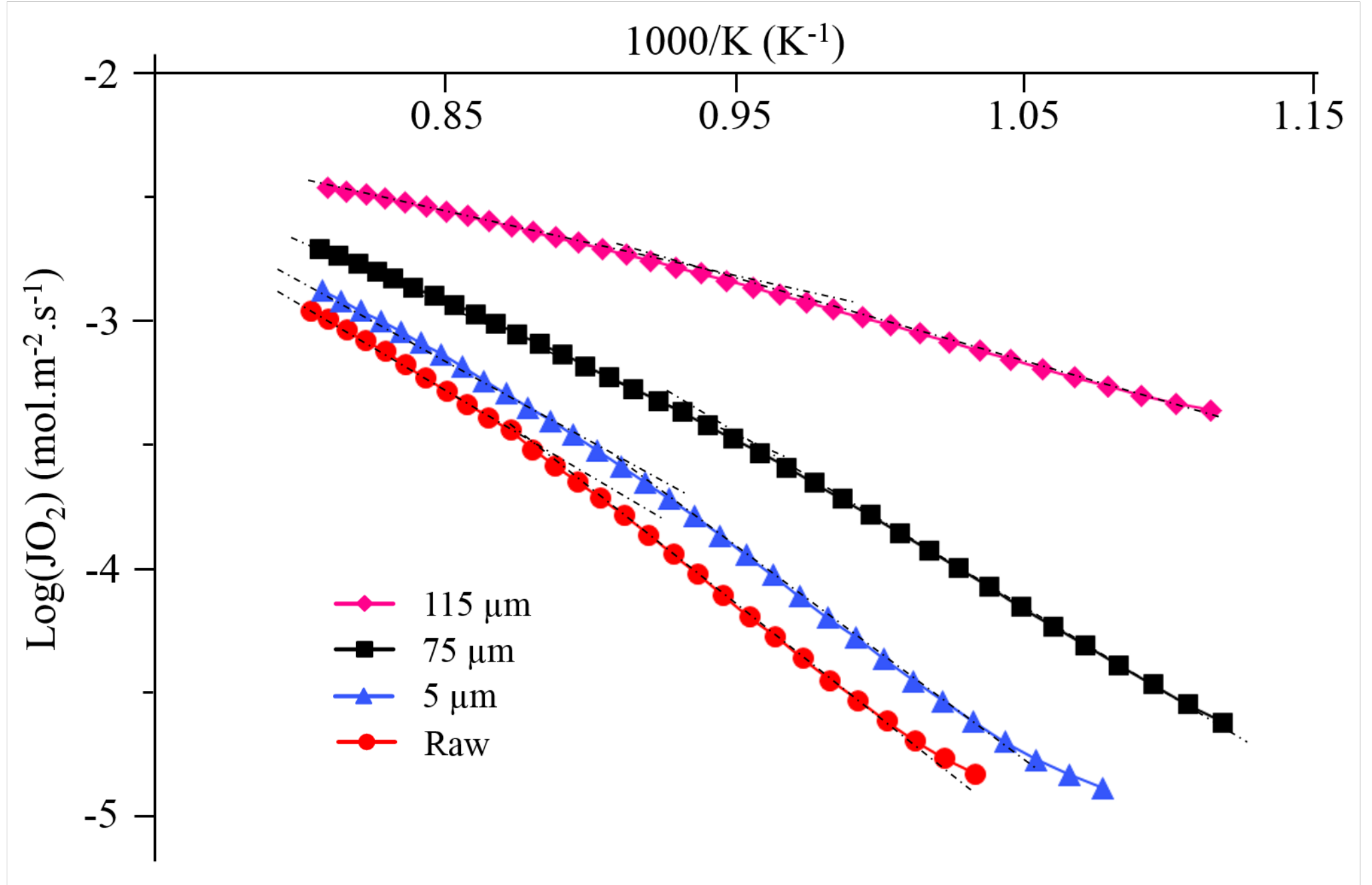
1000/K (K-1)
-2
0.85
0.95
1.05
1.15
Log(JO2) (mol.m-2.s-1)
-3
-4
-5
115 µm
75 µm
5 µm
Raw

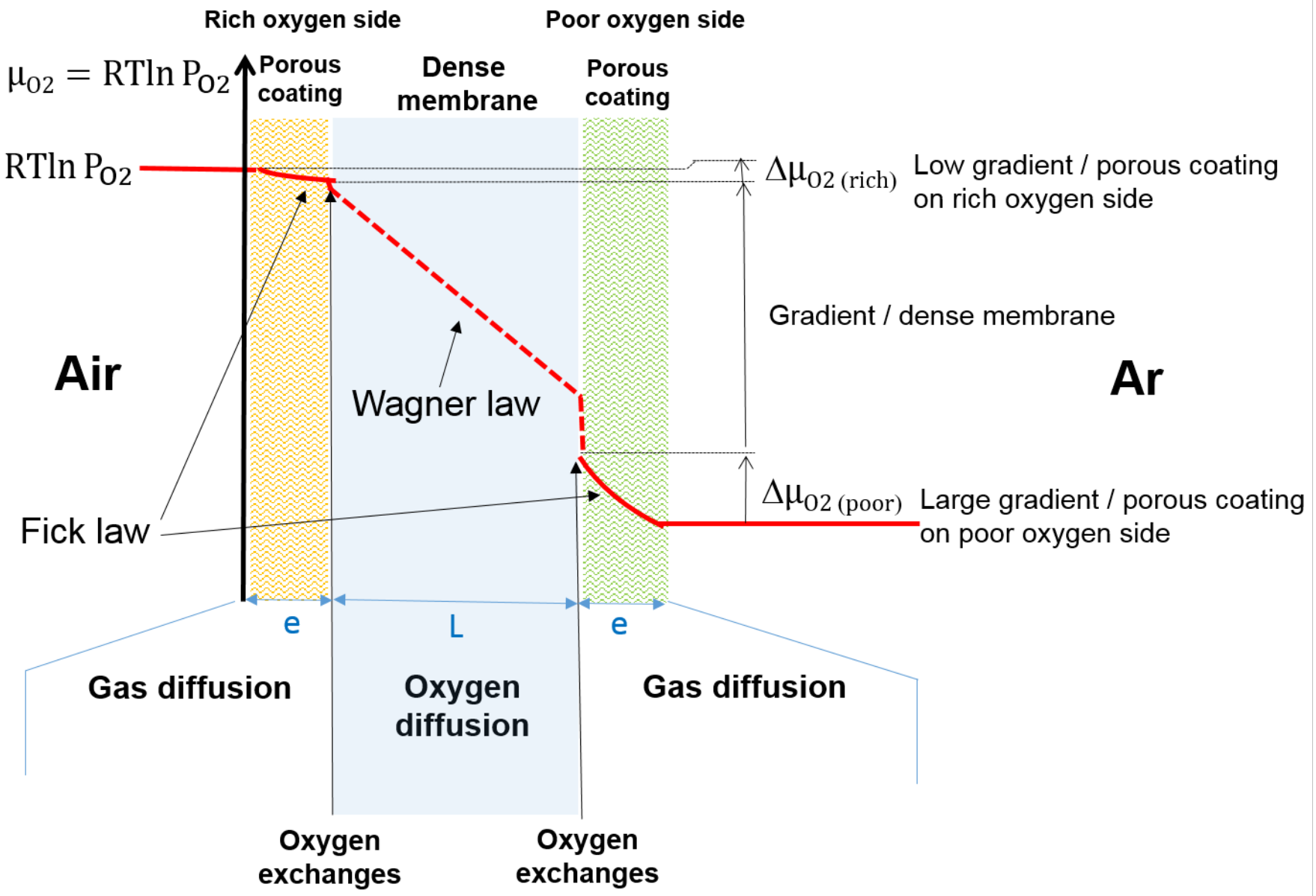
Rich oxygen side
Poor oxygen side
$\mu_{O2} = RT\ln P_{O2}$
Porous coating
Dense membrane
Porous coating
$RT\ln P_{O2}$
$\Delta\mu_{O2\ (rich)}$
Low gradient / porous coating on rich oxygen side
Gradient / dense membrane
Air
Wagner law
Ar
Fick law
$\Delta\mu_{O2\ (poor)}$
Large gradient / porous coating on poor oxygen side
e
L
e
Gas diffusion
Oxygen diffusion
Gas diffusion
Oxygen exchanges
Oxygen exchanges